Available online at www.sciencedirect.com
SCIENCE DIRECT®
ELSEVIER
International Journal of Solids and Structures 43 (2006) 5449–5467
INTERNATIONAL JOURNAL OF SOLIDS and STRUCTURES
www.elsevier.com/locate/ijsolstr

A micromechanical study of residual stress and its effect on transverse failure in polymer–matrix composites

L.G. Zhao *, N.A. Warrior, A.C. Long

School of Mechanical, Materials and Manufacturing Engineering, The University of Nottingham, University Park, Nottingham NG7 2RD, UK

Received 27 April 2005
Available online 3 October 2005

Abstract

Cure residual stress and its effect on damage in unidirectional fibre-reinforced polymer–matrix composites under transverse loading were studied using a micromechanical unit cell model and the finite element method. The overall residual stress introduced from curing was determined by considering two contributions: volume shrinkage of matrix resin from the crosslink polymerization during isothermal curing and thermal contraction of both resin and fibre as a result of cooling from the curing temperature to room temperature. To examine the effect of residual stress on failure, a model based on the Maximum Principal Stress criterion and stiffness degradation technique was used for damage analysis of the unit cell subjected to mechanical loading after curing. Predicted damage initiation and evolution are clearly influenced by the inclusion of residual stress. Residual stress is always detrimental for transverse compressive loading and pure shear loading. For transverse tensile loading, residual stress is detrimental for relatively low resin strength and beneficial for relatively high resin strength. Failure envelopes were obtained for both biaxial normal loading and combined shear and normal loading and the results show that residual stress results in a shifting and contraction of the failure envelopes.

Keywords: Residual stress; Finite element; Curing; Damage evolution; Failure envelopes

1. Introduction

A high temperature curing procedure is generally required for the manufacturing of fibre-reinforced polymer–matrix composites. A typical curing process consists of two steps: (1) isothermal curing at an elevated temperature during which the polymer shrinks as a result of the purely chemical reaction (polymerisation) and builds up stiffness while the reinforcement remains unchanged; (2) thermal cooling from the curing temperature to room temperature during which both polymer and reinforcement contract but by different amount and in addition the polymer may change its stiffness significantly. Chemical shrinkage and thermal cooling contraction of polymer resin are constrained by the surrounding fibre reinforcement, which inevitably results

* Corresponding author. Tel.: +44 115 9513979; fax: +44 115 8466771.
E-mail address: liguo.zhao@nottingham.ac.uk (L.G. Zhao).

0020-7683/$ - see front matter
doi:10.1016/j.ijsolstr.2005.08.012

in the development of residual stresses both at the fibre/matrix interface and inside the bulk resin and fibre. Therefore, cure residual stress is contributed by the chemical shrinkage of the curing resin and the thermal cooling contraction of the resin and fibre system.

Shrinkage stress is a direct result of volume changes of polymer matrix that occur during the polymerization process and will depend on the chemical nature of the material and the curing procedure. During curing, the polymer can go through two main transitions: gelation and vitrification. Gelation corresponds to the formation of molecular networks and vitrification occurs when the glass transition temperature T_g of the polymer reaches the curing temperature. If the material is isothermally cured above the glass transition temperature, only gelation will occur. When the material is cured below the glass transition temperature, it will first gelate and then vitrify. The gelation process results in an equilibrium elastic modulus, whereas vitrification is associated with the transition from a rubbery modulus to a glassy modulus. The change in elastic modulus associated with gelation and vitrification, together with the volume contraction of the polymer, is the dominant factor in the occurrence of the shrinkage stress (Lange et al., 1995).

Thermal cooling stress arises from the mismatch in the coefficients of thermal expansion of the fibre and matrix. During cooling, both constituents contract but the full contraction of the matrix is constrained as a consequence of being bonded to the fibre. On the other hand, the fibre is not only shortened by its own thermal contraction, but is also compressed by the constrained contraction of the matrix. As a result, residual compressive stresses are induced in the fibre. At the same time, the matrix is constrained by the fibre from full contraction, and as a result, is stressed in tension. The magnitude of these stresses will depend on the properties of the fibre and resin system including the thermal expansion coefficient α, Poisson's ratio v and elastic modulus E.

Numerous methods have been developed to determine the residual stresses in polymer–matrix composites both experimentally and analytically. In general, experimental methods fall into two categories, namely destructive and non-destructive methods. Destructive methods, such as hole-drilling (Rendler and Vigness, 1966), sectioning/cutting (Gascoigne, 1994) and first-ply failure test (Kim and Hahn, 1979), require the specimen to be destroyed during testing and therefore cannot be used for in situ measurements. Non-destructive tests include warpage/curvature measurements (Dannenberg, 1965), the cure-reference method (Ifju et al., 2000) and techniques using embedded sensors (strain gauges, fibre optics or crystalline materials) with an X-ray or neutron diffraction method (Kesler et al., 1998; Benedikt et al., 2001). As far as analytical methods are concerned, residual stresses in composites are generally studied on the macro- and meso/microlevels. On the macro-level, classical laminate theory is generally used and gives predictions at the ply level (Stone et al., 1997; Olivier and Cottu, 1998; Gopal et al., 2000). On the meso/microlevel, the unit cell or representative volume element (RVE) approach based on the meso/microscopic periodic structure of the laminate is generally adopted and the analysis is often carried out using a numerical procedure such as the finite element method (Andersson et al., 2000; Sweeting and Thomson, 2004; Zhang et al., 2004). Residual stress and strain fields at the fibre–matrix or tow level can be predicted from the meso/microscopic unit cell model.

The formation of residual stresses, especially the tensile stress in the matrix, is generally detrimental in the production of polymer–matrix composite parts, since the stress can be high enough to initiate material damage before loading such as interface debonding and matrix microcracking as shown in Fig. 1 (Gentz et al., 2004a,b). The initial damage can reduce the stiffness and the strength of the material, as well as acting as sites for environmental degradation and nucleation of macrocracks. Therefore, any analytical or experimental study involving damage and fracture mechanics of composites should take into account residual stresses if they exist. On the other hand, some residual stress states may be favourable; for example, positive hoop stresses around the reinforcing fibre may augment the pull-out energy dissipation and thus increase toughness (Nimmer, 1990).

Although residual stress has been extensively studied in polymer–matrix composites, most work focused on the determination of residual stress due to the thermal mismatch of the fibre and matrix system. Also, effects of residual stress on failure of composites have not been deeply addressed yet, especially the effect on failure envelopes for biaxial loading. In this work, finite element analysis was used to study the residual stress and its effect on transverse failure of unidirectional fibre-reinforced polymer–matrix composites using a micromechanical unit cell model. The residual stress introduced during curing was determined by considering the contributions from both the chemical shrinkage of resin and the thermal cooling contraction of fibre and resin. Effects of

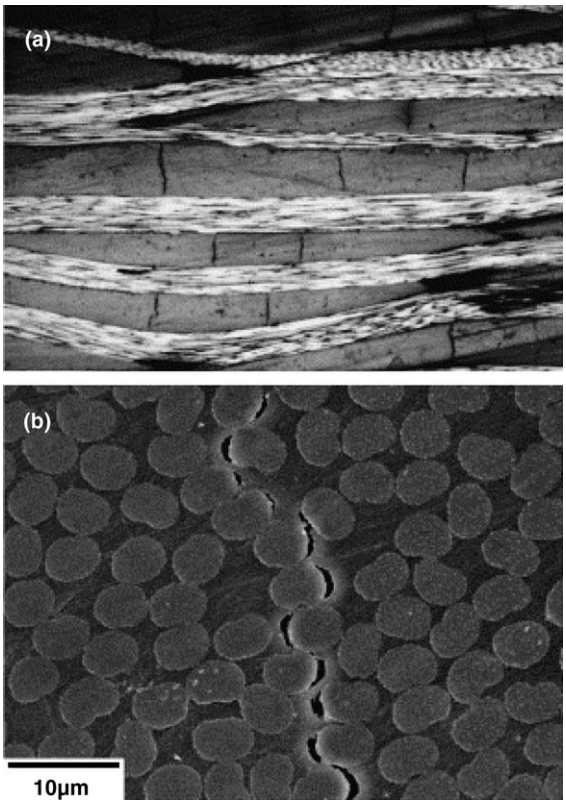

Fig. 1. Transverse tow microcracks in a woven graphite fibre polyimide composite prior to loading (from Gentz et al., 2004a,b).

residual stress on damage evolution and failure of the unit cell subjected to transverse mechanical loading after curing were predicted using the Maximum Principal Stress failure criterion and the post-failure stiffness reduction technique. Transverse mechanical loading was applied to the unit cell model by specifying uniform displacements along the edges of the unit cell. Uniaxial tension and compression and pure shear were all considered, where appropriate boundary conditions and constraints were required for each loading case. Furthermore, biaxial normal loading and combined shear and normal loading are applied to the model to study the effect of residual stress on failure envelopes.

2. Finite element modelling

2.1. Micromechanical model

In unidirectional fibre composites, the actual fibre distribution is quite random across the cross-section. For simplicity, most micromechanical models assume a periodic arrangement of fibres for which a unit cell can be isolated. The unit cell has the same elastic constants and fibre volume fraction as the composite. The periodic fibre sequences commonly used are the square and hexagonal arrays. Here the square array is considered for the residual stress analysis as shown in Fig. 2 and the matrix is assumed to be perfectly bonded to the fibres throughout the analysis.

Two micromechanical models are constructed depending on the type of load applied after curing. For transverse normal loading, due to the symmetry only a quarter of the unit cell (Fig. 3a) is considered. Boundary conditions used for the model are illustrated in Fig. 3a, where equal x-displacement and y-displacement are required for the right and top edges, respectively. For transverse shear loading or combined normal and shear loading, a whole unit cell (Fig. 3b and c) is considered here. It should be pointed out that a quarter

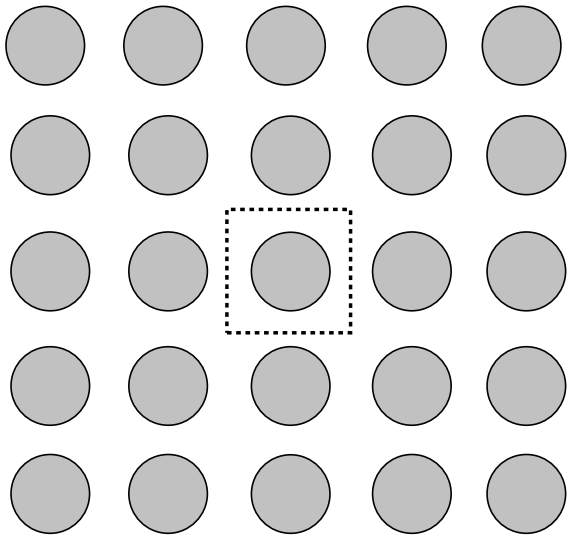

Fig. 2. Schematics of square fibre arrays and the representation volume element or unit cell (enclosed by dashed lines).

unit cell can also be used to simulate the transverse shear deformation by considering appropriate boundary and symmetry conditions as shown in Yuan et al. (1997). However, the adoption of a whole unit cell in the present work can facilitate the application of multi-point constraints for finite element shear deformation analysis (ABAQUS, 2005). Boundary conditions used for residual stress analysis of the whole unit cell are shown in Fig. 3b, together with the following kinematic constraints:

$$u(a,y) - u(-a,y) = u(E) - u(F), \tag{1}$$

$$v(x,b) - v(x,-b) = v(G) - v(F), \tag{2}$$

where $u(E)$ and $u(F)$ are the x-direction displacements of node E and node F, and $v(G)$ and $v(F)$ are the y-direction displacements of node G and node F.

In order to satisfy the deformation requirements for shear loading or combined normal and shear loading applied after curing, boundary conditions need to be modified (Sun and Vaidya, 1996). Fig. 3c shows the modified boundary conditions for which the kinematic constraints given by (1) and (2) are still valid.

To simulate the shear loading, a constant displacement δ_x along the x-axis is applied to the top and bottom surfaces of the unit cell but in the opposite directions and expressed as

$$u(x,b) = -u(x,-b) = \delta_x. \tag{3}$$

In this case, the equivalent shear strain is obtained as

$$\varepsilon_{xy} = \frac{\delta_x}{2b}. \tag{4}$$

In addition, to simulate the normal loading in the y-direction, a constant displacement δ_y in the y-direction is applied at the two top corners of the whole unit cell, together with the following kinematic constraints for the right and left edges (Sun and Vaidya, 1996),

$$v(a,y) = v(-a,y). \tag{5}$$

The equivalent normal strain in the y-direction is then obtained as

$$\varepsilon_{yy} = \frac{\delta_y}{2b}, \tag{6}$$

where if $\delta_y = 0$, a pure shear deformation will be realized (Sun and Vaidya, 1996).

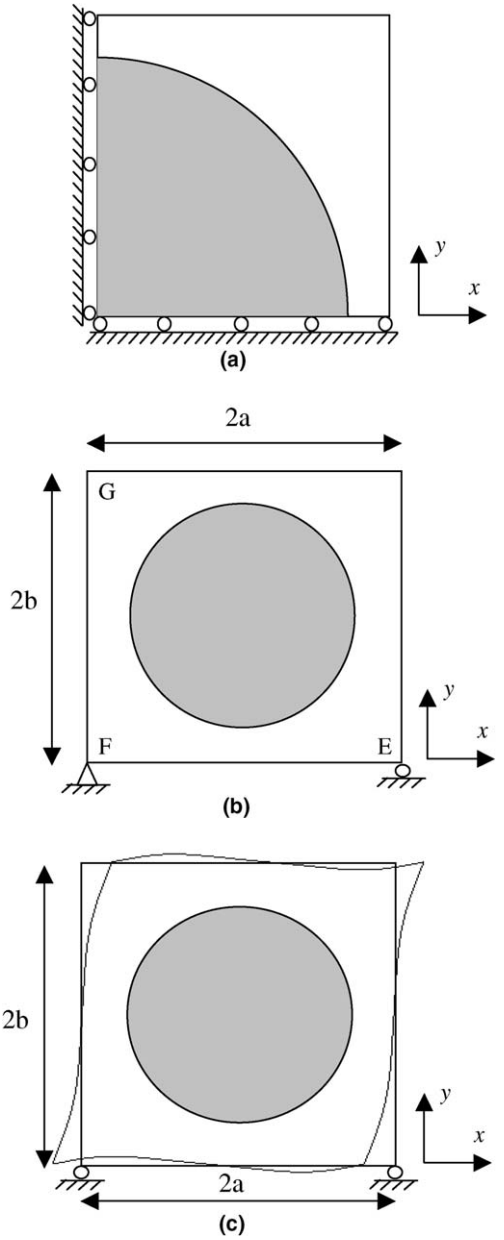

Fig. 3. Illustration of model boundary conditions: (a) a quarter of unit cell, (b) the whole unit cell for residual stress analysis and (c) the whole unit cell for shear loading after curing.

Following the above constraints, the predicted deformed shape for pure shear loading is illustrated in Fig. 3c and agrees with that in Sun and Vaidya (1996). The meshes generated for the two models are shown in Fig. 4 where the volume fraction is taken to be 60% and 6-noded plane strain elements are used. The number of elements is approximately 6000 for the quarter unit cell model and 24,000 for the whole unit cell model. The average element size within the fine mesh region is around 0.01 times the fibre radius. Mesh sensitivity analysis suggests that the mesh shown in Fig. 4 is fine enough to produce quite accurate results compared to a doubly refined mesh, with a difference within 0.2% in terms of residual stress and failure strain level.

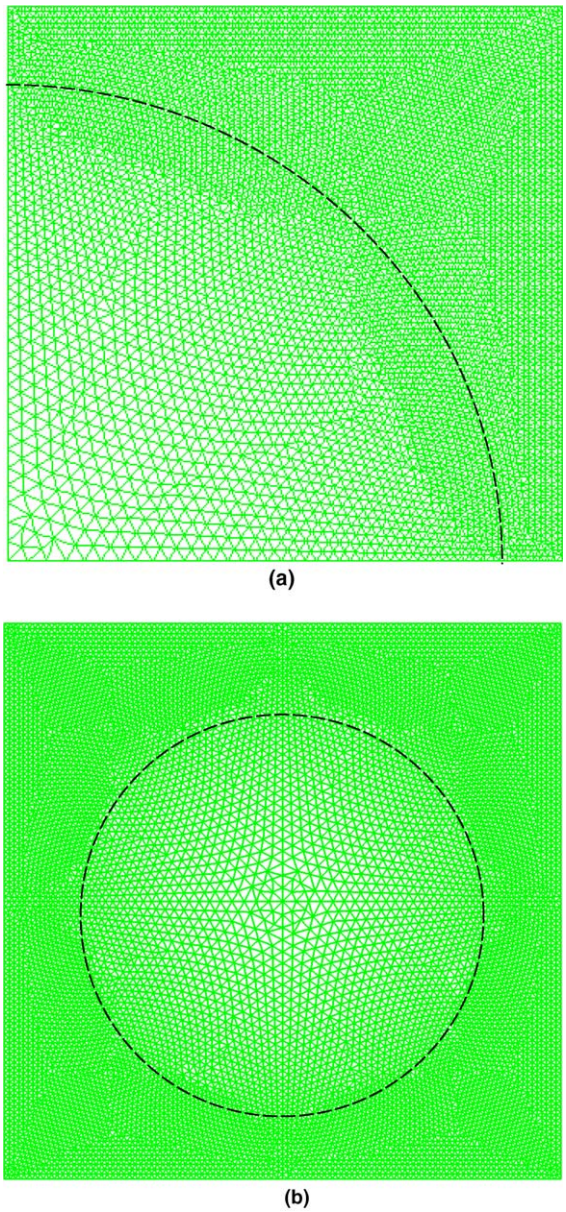

Fig. 4. Finite element mesh: (a) a quarter of unit cell used for subsequent normal loading analysis and (b) a whole unit cell used for subsequent shear loading analysis.

2.2. Residual stress analysis

For constrained shrinkage and thermal cooling contraction of the resin, the total induced strain can be expressed as

$$d\varepsilon_{ij} = de_{ij} + \delta_{ij}\, ds + \delta_{ij}\alpha(T)\, dT, \tag{7}$$

where $d\varepsilon_{ij}$ is the total strain increment, de_{ij} the elastic strain increment, ds the free shrinkage strain increment due to the chemical reaction (cross-linking) in the absence of constraint, $\alpha(T)$ the thermal expansion coefficient which is dependent on the temperature, and dT the temperature change.

From Eq. (7), the stress–strain relationship can be derived as

$$d\sigma_{ij} = C_{ijkl}\, de_{kl} = C_{ijkl}\{d\varepsilon_{ij} - \delta_{ij}\, ds - \delta_{ij}\alpha(T)\, dT\}, \tag{8}$$

where $d\sigma_{ij}$ are the stress increments and C_{ijkl} the stiffness components. The above stress analysis is based on linear elasticity and the stiffness components C_{ijkl} are related to the Young's modulus E and the Poisson's ratio v of the material.

Eq. (8) was derived for the residual stress analysis in the resin. For isotropic fibre, Eq. (8) is still applicable by simply ignoring the chemical shrinkage strain.

2.3. Material

The composite constituents considered here are glass fibre and epoxy resin, whose properties are given in Zhang et al. (2004). The properties of glass fibre are assumed to remain constant and independent of the temperature change with Young's modulus $E = 72.5$ GPa and Poisson's ratio $v = 0.22$ and the coefficient of thermal expansion $\alpha = 5.0 \times 10^{-6}/°C$. However, for the epoxy resin, thermal transition temperatures, for example, the glass transition temperature T_g, strongly affect mechanical properties. Therefore, the material properties of the resin were proposed as a function of temperature in Zhang et al. (2004), which was also used throughout the present analysis and summarized as follows:

(a) Poisson's ratio is assumed to be temperature independent with a value of $v = 0.4$.

(b) To consider the change of Young's modulus E over the temperature range from curing to room temperature, the total temperature range was divided into three regions linked to the glass transition temperature T_g. The transition region around T_g is assumed to be $T_g - \Delta T_1 \leqslant T \leqslant T_g + \Delta T_2$, where E varies greatly. For $T \geqslant T_g + \Delta T$, the matrix is in liquid or rubbery state and E has a very small value. When $T \leqslant T_g - \Delta T_1$, the matrix is in solid state and E changes only slightly. For each region, the modulus is obtained by the following proposed functions,

$$E(T) = E(T_r)\exp\left(-k_1 \frac{T - T_r}{T_g - \Delta T_1 - T_r}\right) \quad T \leqslant T_g - \Delta T_1, \tag{9}$$

$$E(T) = E(T_g - \Delta T_1)\exp\left(-k_2 \frac{T - T_g + \Delta T_1}{\Delta T_1 + \Delta T_2}\right) \quad T_g - \Delta T_1 \leqslant T \leqslant T_g + \Delta T_2, \tag{10}$$

$$E(T) = 0.01E(T_r) \quad T \geqslant T_g + \Delta T_2, \tag{11}$$

where the constants are determined by Zhang et al. (2004) with $T_g = 110$ °C, $T_r = 23$ °C, $\Delta T_1 = \Delta T_2 = 35$ °C, $E(T_r) = 2600$ MPa, $E(T_g - \Delta T_1) = 0.7E(T_r)$, $E(T_g + \Delta T_2) = 0.01E(T_r)$, $k_1 = 0.357$ and $k_2 = 4.249$.

(c) The thermal expansion coefficient α is assumed to change linearly with the temperature with a slope of

$$K = \frac{\alpha_l - \alpha(T_r)}{T_g - T_r}, \tag{12}$$

where $\alpha(T_r) = 63 \times 10^{-6}/°C$ and $\alpha_l = 139 \times 10^{-6}/°C$.

The isothermal curing reaction of a thermoset resin involves dramatic changes in the properties of the resin. After heating of the initially liquid monomer, the chemical reaction commences. The molecular weight and the degree of crosslinking increase and the volume of the system decreases. As the reaction proceeds two phenomena may occur independently: gelation and vitrification. Gelation corresponds to the formation of a molecular network and can be regarded as the point after which the system can sustain stress. Vitrification occurs when the glass transition temperature T_g of the reacting system reaches the cure temperature. On vitrification the system, either a rubbery network or a viscous liquid (if vitrification precedes gelation), is transformed into a glassy state. The property change was shown to be closely related to the degree of cure of the resin (Stone et al., 2000; Flores et al., 2002). Here, the properties of the resin were assumed to be independent of the degree of cure and constant at the isothermal curing temperature. Their values were obtained from the temperature-dependent functions (9)–(11) and used for the shrinkage residual stress analysis in the present work. This

assumption was justified by the fact that the modulus was built up very quickly after resin gelation or vitrification (Lange et al., 1995). Also stress relaxation due to the viscoelasticity of the epoxy resin (Kim and White, 1998; Zhang et al., 2004) was ignored here, and the epoxy was treated as linear elastic.

3. Damage prediction

As shown in Fig. 2, at the microscale the model consists of fibre reinforcement and resin matrix. Both fibre and resin are isotropic materials and the Maximum Principal Stress theory is applicable for damage onset prediction. If the stress level satisfies the failure criterion, the fibre or matrix would crack. Final failure corresponds to the rupture of the unit cell, which is unable to carry further load. The Maximum Principal Stress failure criterion is summarized as

$$\sigma_{\max} \geqslant \sigma_u^{\mathrm{t}}, \tag{13}$$

$$\sigma_{\min} \leqslant \sigma_u^{\mathrm{c}}, \tag{14}$$

where $\sigma_{\max}$ and $\sigma_{\min}$ are the maximum and minimum principal stresses and σ_u^{t} and σ_u^{c} are the tensile and compressive strengths of the material, respectively.

It is a common practice in simulating material damage to reduce the stiffness (or stiffness in a certain direction) to a near zero value following the onset of damage. Selective and non-selective stiffness reduction schemes are often used. Selective schemes are typically applied for composites where the load-carrying nature is dependent on the damage orientation (Blackketter et al., 1993). For isotropic material, damage is independent of the material orientation, so that non-selective stiffness reduction is applied. In this case, once the failure criterion is satisfied, the moduli are reduced to near zero values (0.01 times the original value), including the shear modulus.

The non-selective stiffness degradation scheme, together with the residual stress analysis from Eq. (8), was programmed into a user-defined material subroutine (UMAT) interfaced with the commercial finite element code ABAQUS standard (ABAQUS, 2005). During the analysis, the stress level was calculated at the Gauss integration points for each time increment and examined for damage detection using the Maximum Principal Stress failure criterion. Once the failure criterion was satisfied, the stiffness reduction was applied for further analysis until final failure of the model. The damage model is similar to that used in Zhao et al. (in press) for damage progression analysis in an E-glass/vinylester non-crimp fabric composite laminate.

4. Results and discussion

Since transverse failure of composites is related to the (x,y) in-plane stress state, in the following distributions of the maximum in-plane principal residual stress are presented and predictions for transverse failure are also based on the maximum in-plane principal stress.

4.1. Residual stress

As discussed above, residual stress has two parts: the chemical shrinkage residual stress and the thermal cooling residual stress. The analysis was performed by two discrete steps, where step one is the shrinkage stress analysis and step two is the thermal cooling stress analysis. The shrinkage residual stress was calculated by a given amount of resin shrinkage. For the epoxy resin considered here, the shrinkage strain was chosen to be between 0.5% and 2%, which corresponds to the volume change between 1.5% and 6% and falls within experimental measurements (Russell, 1993; Oota and Saka, 2001; Li et al., 2004; Sakaguchi et al., 2004). The thermal residual stress is due to the cooling of the system from the curing temperature to room temperature 23 °C. Finite element analysis was carried out incrementally in each step. In step one, the total shrinkage strain was applied to the resin incrementally and the residual stress was calculated through the constitutive Eqs. (7) and (8). In step two, the shrinkage strain for the resin was set to be zero and only the thermal cooling contraction was considered for residual stress calculation from Eqs. (7) and (8).

Analysis was first given to the situation of 1% shrinkage strain and 100 °C curing temperature. The considered curing temperature is slightly below the glass transition temperature 110 °C of the epoxy resin (Zhang et al., 2004). A contour plot of the obtained maximum principal residual stress is shown in Fig. 5. It can be seen that, as expected, the resin experiences a tensile maximum principal residual stress while the fibre has a compressive maximum principal residual stress. The maximum principal residual stress has greatest value (32.5 MPa) at the middle area of the interface between the resin and the fibre but within the resin.

The distribution of the resin's maximum principal residual stress along the interface is presented in Fig. 6 for the situation of 1% shrinkage strain and 100 °C curing temperature, where the shrinkage and thermal cooling contributions are shown separately. Compared to the chemical shrinkage of resin, the thermal cooling contribution seems dominant for 100 °C curing temperature. The relatively small contribution from the chemical shrinkage is due to the low resin modulus at 100 °C curing temperature.

For 100 °C curing temperature, Fig. 7a shows the distribution of the resin's maximum principal residual stress along the interface for three given shrinkage strains, i.e., 0.5%, 1% and 2%, respectively. The higher the shrinkage strain, the higher the residual stress. With 0.5% shrinkage strain, the residual stress distribution was shown in Fig. 7b for three curing temperatures, i.e., 80 °C, 100 °C and 120 °C, respectively. It can be seen that for a given amount of chemical shrinkage, the lower the curing temperature the higher the overall residual stress. This is due to the more significant contribution from the chemical shrinkage residual stress at lower curing temperature, a direct result of higher modulus at lower curing temperature.

According to the Maximum Principal Stress failure criterion, the residual stress can introduce resin failure along the interface of the fibre and the resin, which agrees with the experimental observation of microcracking

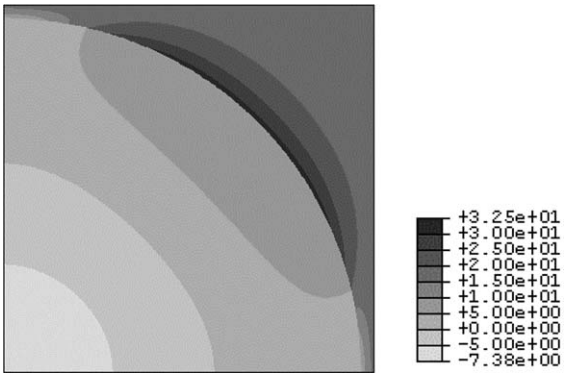

Fig. 5. Contour plot of the maximum principal residual stress (MPa) for 1% shrinkage strain and 100 °C curing temperature.

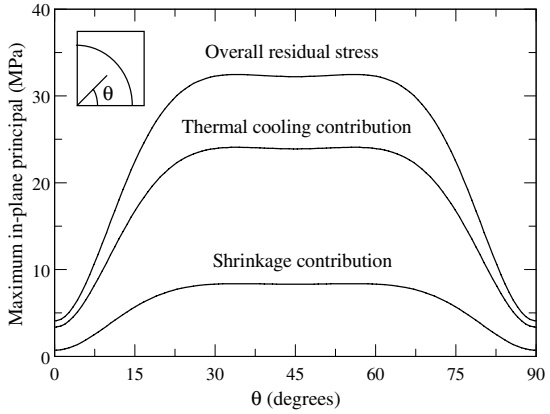

Fig. 6. Distribution of the maximum principal residual stress in the rein along the fibre/matrix interface for 1% shrinkage strain and 100 °C curing temperature.

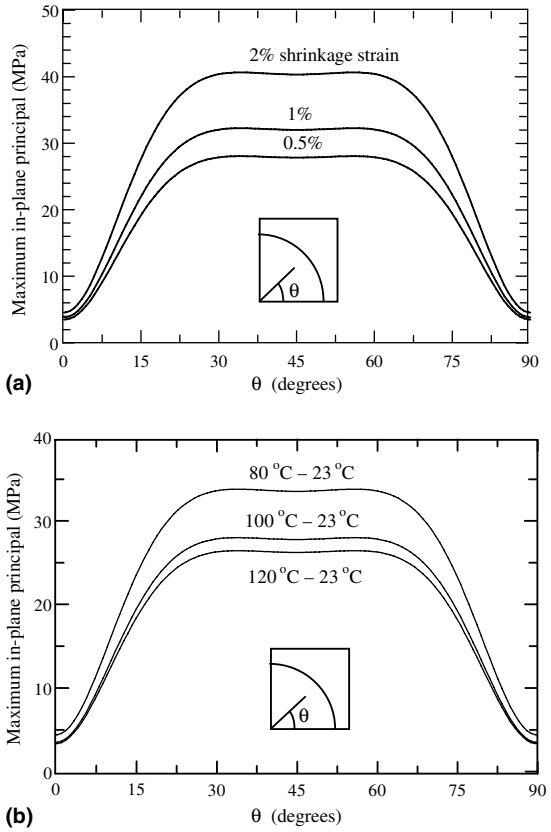

Fig. 7. Distribution of the maximum principal residual stress in the resin along the fibre/matrix interface: (a) varying shrinkage strain at 100 °C curing temperature and (b) varying curing temperature at 0.5% shrinkage strain.

shown in Fig. 1 (Gentz et al., 2004a,b). In most published work on residual stress, thermal cooling was treated as the main source of residual stress in composites (Sweeting and Thomson, 2004; Zhang et al., 2004; Olivier and Cottu, 1998). This method excludes the shrinkage residual stress developed during isothermal curing and thus underestimates the overall residual stress. Therefore the residual stress from thermal cooling can be understood as the lower bound of the overall residual stress. From Fig. 6, it seems that curing shrinkage makes a reasonable contribution to the overall residual stress and should be included for stress analysis in polymer composites.

4.2. Effect of residual stress on transverse failure

To study the influence of residual stress/strain on the response of the unit cell model, the damage evolution in the matrix was examined under transverse loading. After curing and thermal cooling analysis, a global strain is applied to the model which is achieved by specifying a uniform displacement at the model surfaces. The global strain is applied up to 2% and within small strain scope. At each time increment of the analysis, the extent of damage zone in the matrix is determined using the Maximum Principal Stress failure criterion. Throughout the following analyses, the fibre shows no sign of damage due to its high strength (Soden et al., 1998). Therefore, damage and failure are referred to the matrix only.

4.2.1. Uniaxial tensile loading

With the residual stress/strain state, the evolution of damage for uniaxial tensile loading in the x-direction is shown in Fig. 8a where the damage zone is represented by a black shading in the matrix. The tensile strength of the epoxy resin is taken to be 80 MPa (Soden et al., 1998) and the residual stress/strain state corresponds to

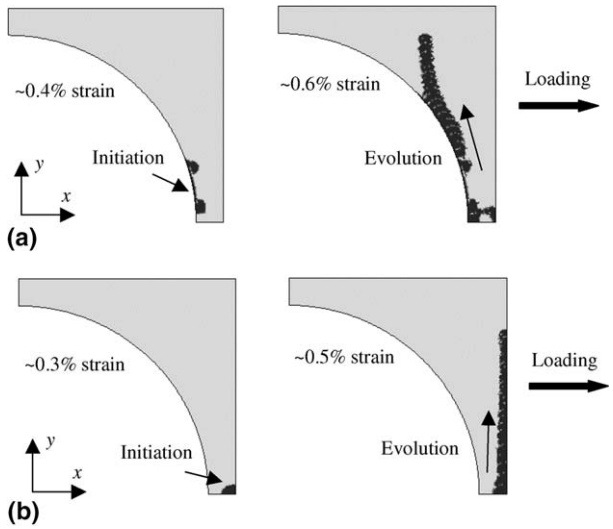

Fig. 8. Damage initiation and evolution under uniaxial transverse tensile loading (up to 1% global strain): (a) with residual stress and (b) no residual stress.

the situation of 1% shrinkage strain and 100 °C curing temperature. For a comparison, Fig. 8b shows the damage evolution under the same uniaxial tensile loading but neglecting the residual stress/strain introduced during the curing process. It can be seen that the site of damage initiation and the subsequent evolution are clearly affected by considering the residual stress (Asp et al., 1996; Kwon and Berner, 1997; Zhang et al., 1998, 2004). Without residual stress, damage initiates at the right-bottom corner and propagates upwards along the right edge. If the residual stress is included, damage would initiate near the bottom of the fibre/matrix interface and propagate upwards along the interface.

During the above damage analysis, the global stress–strain response in the loading direction was monitored and the results are given in Fig. 9 for the cases with and without residual stress. For both cases, the carried stress starts to drop quickly and significantly from the start of damage initiation. Since the damage prediction is based on the stiffness reduction technique, the model is expected to have some degraded stiffness after damage initiation and thus exhibits some branches in the global stress–strain traces with further load increase (see Figs. 9, 12a and 14a). Different branching behaviour in the global stress–strain trace was also noticed for the cases with and without residual stress, which might be due to the difference of the degraded stiffness for each case. No matter how different the branching behaviour is for each case, the global stress–strain traces

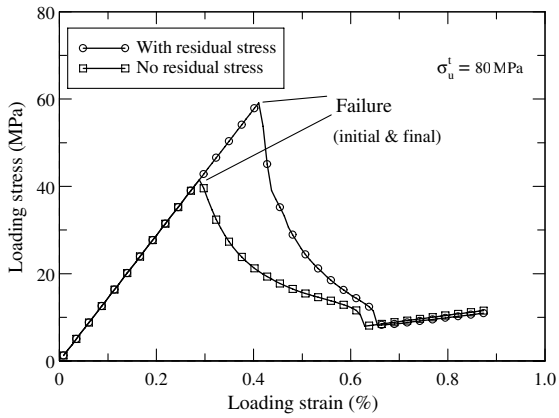

Fig. 9. Global stress–strain trace in the x-direction for uniaxial transverse tensile loading.

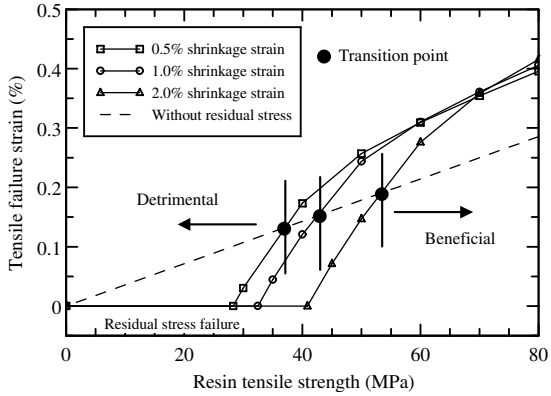

Fig. 10. Failure strain as a function of the resin tensile strength under uniaxial transverse tensile loading.

consistently show that once the damage is initiated, the model is unable to carry the applied load and tends to fail quickly. Thus, the initial failure strain level is also the final failure level for transverse loading.

The obtained failure strain is plotted in Fig. 10 as a function of the resin tensile strength, where three residual stress/strain states were considered by varying the amount of shrinkage strain from 0.5% to 2% at 100 °C curing temperature. The dashed line shows the result for the case without residual stress. Clearly, the effect of residual stress on damage depends on two factors: the magnitude of the residual stress and the strength of resin. If the residual stress exceeds the resin strength, failure occurs before any load application (Lennon and Prendergast, 2002). If the resin has a high strength, then there is a transition point at which the curve with residual stress intersects the curve without residual stress. On the left of the transition point, the residual stress tends to cause failure earlier and thus plays a detrimental role. On the right of the transition point, the residual stress delays the occurrence of failure and appears to be beneficial. The transition point varies with the residual stress/strain state. Severe residual stress shifts the transition point to the right and needs higher resin strength for a beneficial effect.

The benefits of residual stress beyond the transition point can be explained by the stress profiles plotted in Fig. 11. When no residual stress was considered, the maximum principal stress has the greatest positive value at position A with a direction along the x-axis (Fig. 11b) which will introduce initial failure at position A (see Fig. 8b). Looking at the residual stress in the x-direction, it is found that a negative value (−36.1 MPa for 1% shrinkage strain and 100 °C curing temperature) exists at position A (Fig. 11a). The negative residual stress at position A in the x-direction would postpone the occurrence of failure by negating part of the tensile maximum principal stress at position A (Fig. 11b) through superposition, thus bringing a beneficial effect. Accompanying this beneficial effect, damage initiation and evolution along the right edge for no residual stress (Fig. 8b) was switched to along the fibre–matrix interface when the residual stress is included (Fig. 8a).

4.2.2. Uniaxial compressive loading

For uniaxial compressive loading in the x-direction, damage evolution patterns exhibit the behaviour similar to that shown in Fig. 8b. In this case, analyses show that the residual stress does not influence the site of damage initiation and the pattern of damage evolution. Damage always initiates at the right-bottom corner (see Fig. 8b) and grows along the right edge irrespective of the residual stress. The cause of failure was due to the compressive minimum principal stress which reaches the resin compressive strength.

Under uniaxial compressive loading, the monitored global stress–strain trace during the damage analysis is given in Fig. 12a where the compressive strength of the epoxy resin is taken to be 160 MPa (Soden et al., 1998). The trace with residual stress is obtained by considering 1% shrinkage strain and 100 °C curing temperature. As shown in Fig. 12a, the carried stress starts to drop from the point of damage initiation and, as for the tensile loading, the initial failure strain level is also the final failure level. The compressive failure strain is plotted in Fig. 12b as a function of resin compressive strength for three different amounts of shrinkage strain (0.5%, 1% and 2%) at 100 °C curing temperature. The dashed line represents the case without residual stress. It can be

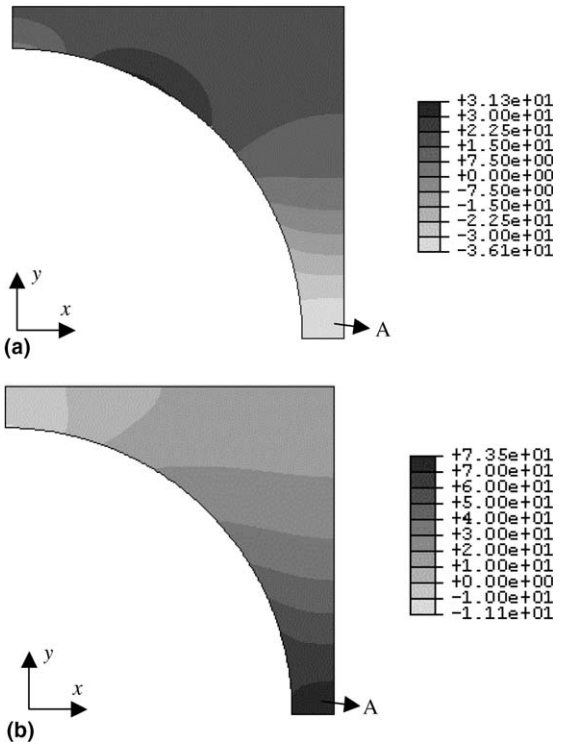

Fig. 11. Stress contours (MPa): (a) residual stress in the x-direction (1% shrinkage strain and 100 °C curing temperature) and (b) the maximum principal stress at an x-direction global strain of ~0.3% (no residual stress).

seen that, although residual stress does not affect the damage pattern, it does cause earlier failure and plays a detrimental role for compressive loading. Again, this is due to the influence of negative residual stress at position A in the x-direction (Fig. 11a). The negative residual stress would facilitate the occurrence of failure by enhancing the compressive minimum principal stress at position A under compressive loading, thus having a detrimental effect.

4.2.3. Pure shear loading

Initiation and evolution of damage for pure shear loading are shown in Fig. 13a for the case with residual stress (1% shrinkage strain and 100 °C curing temperature) and Fig. 13b for the case without residual stress. Failure is due to the tensile maximum principal stress which reaches the resin tensile strength 80 MPa. It can be seen that under pure shear loading, damage evolution is mainly along the interface, initiating simultaneously near the vertical and horizontal areas of the interface and growing towards each other as shown in Fig. 13a and b. The site of damage initiation and the subsequent evolution are not so affected by the residual stress.

Fig. 14a shows the global shear stress–strain trace for pure shear loading. The initial failure point is the final failure point for both the case without residual stress and the case with residual stress (1% shrinkage strain and 100 °C curing temperature). As for transverse tensile and compressive loading (Figs. 9 and 12a), the carried stress starts to drop at the point of damage initiation where the tensile maximum principal stress reaches the resin tensile strength (80 MPa). The shear failure strain is plotted in Fig. 14b as a function of resin tensile strength where three different levels of shrinkage strain (0.5%, 1% and 2%) at 100 °C curing temperature were considered. Compared to the result for the case without residual stress, it can be seen that residual stress causes earlier failure and plays a detrimental role for shear loading. This is because of the tensile maximum principal residual stress along the fibre–matrix interface which facilitates the initiation and progress of damage (Fig. 13a and b) along the fibre/matrix interface under shear loading.

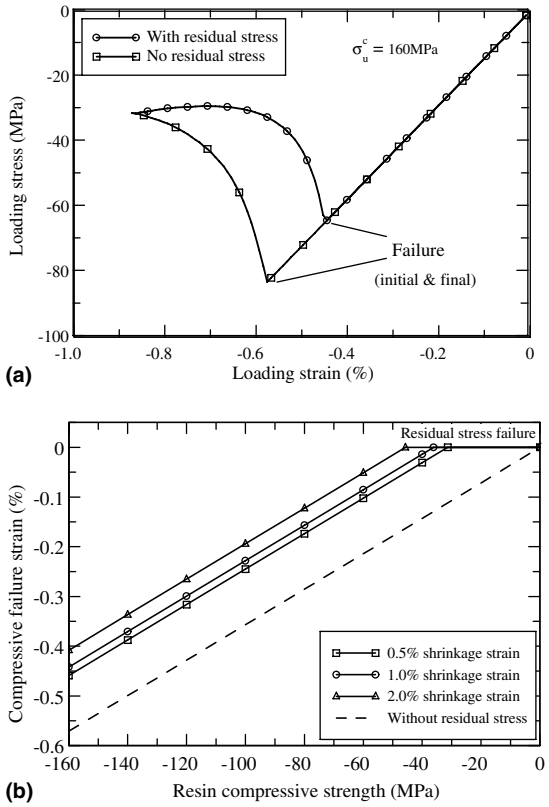

Fig. 12. (a) Global stress–strain trace in the x-direction and (b) failure strain as a function of the resin compressive strength for uniaxial transverse compressive loading.

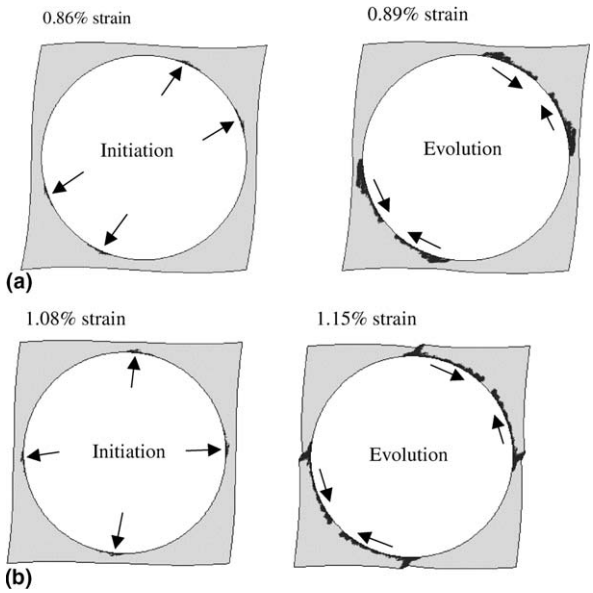

Fig. 13. Damage initiation and evolution under pure shear loading (up to 2% global strain): (a) with residual stress and (b) no residual stress.

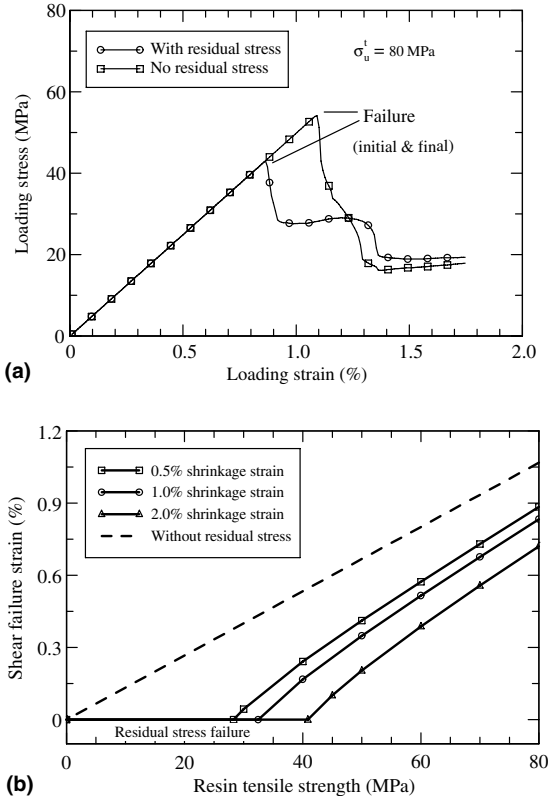

Fig. 14. (a) Global stress–strain trace in the x-direction and (b) failure strain as a function of the resin tensile strength for pure shear loading.

4.2.4. Biaxial normal loading

Under biaxial normal loading, failure envelopes were constructed by considering different biaxial strain ratios and the results are shown in Fig. 15a and b for two selected resin strengths. Note that the compressive strength was taken to be twice the tensile strength for the epoxy resin (Soden et al., 1998) and the considered residual stress/strain state corresponds to 1% shrinkage strain and 100 °C curing temperature. Failure envelopes for no residual stress are also included for comparison. For the case without residual stress, the shape of failure envelope is more or less a square which is consistent with the Maximum Principal Stress failure criterion. By considering the residual stress, transverse failure envelopes for biaxial normal loading are shown to be shifted and contracted from those derived by excluding residual stress. Similar shifting effect of residual stress on initial yield surfaces was reported by Aghdam and Khojeh (2003) for unidirectional fibre-reinforced metal–matrix composites under transverse loading.

From the failure envelopes, residual stress is shown to be detrimental for compression dominated loading by causing earlier failure. On the other hand, for tension dominated loading residual stress has a complex effect depending on the magnitude of the residual stress and the resin strength. As shown in Fig. 15a, for relatively low resin strength residual stress brings earlier failure and has a detrimental effect. For relatively high resin strength, residual stress delays failure and appears to be beneficial as shown in Fig. 15b. This is attributed to the influence of negative residual stress both at the right-bottom corner of the quarter unit cell in the x-direction (Fig. 11a) and at the left-top corner of the quarter unit cell in the y-direction. Contour plot of the residual stress in the y-direction can be obtained by simply exchanging the x-axis and the y-axis in Fig. 11a. Therefore, the residual stress in the y-direction has negative value at the left-top corner of the quarter unit cell.

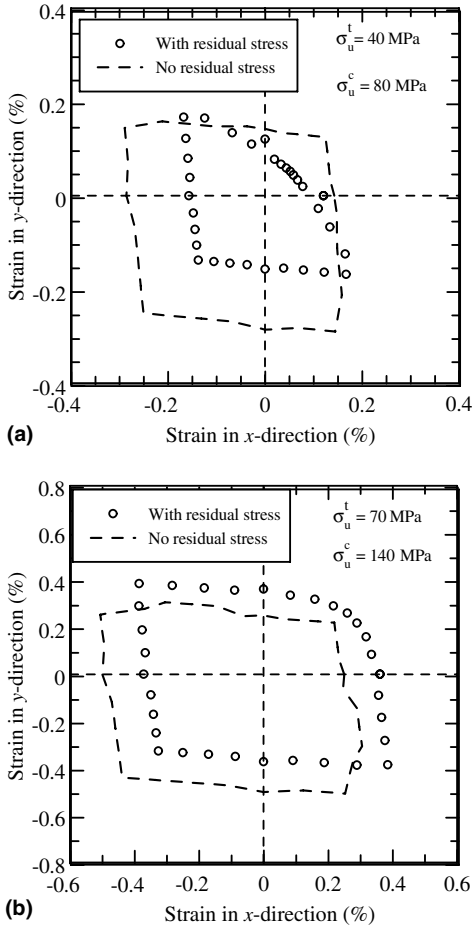

Fig. 15. Failure envelopes for biaxial transverse normal loading: (a) $\sigma_u^c = 2\sigma_u^t = 80$ MPa and (b) $\sigma_u^c = 2\sigma_u^t = 140$ MPa.

4.2.5. Combined shear and normal loading

With two selected resin strengths, failure envelopes for combined shear and normal loading are given in Fig. 16a and b where the normal loading is applied in the *y*-direction. Again, the compressive strength was chosen to be twice the tensile strength for the epoxy resin (Soden et al., 1998). By the inclusion of residual stress (1% shrinkage strain and 100 °C curing temperature), transverse failure envelopes for combined shear and normal loading are also shown to be shifted and contracted from those derived by ignoring the residual stress. Experiments on biaxial failure envelopes for unidirectional fibre composites have focused on the combined longitudinal and transverse loading conditions (see Soden et al., 2002). Due to the lack of test data on transverse failure envelopes, comparison of the present results with experimental data is not included in this work. However, further analysis on failure envelopes is ongoing for combined longitudinal and transverse loading using a three-dimensional micromechanical model and the results are expected to be compared with experimental measurements.

As seen in Fig. 16a and b, in most cases residual stress is shown to be detrimental for combined shear and normal loading. This is due to the combined influence of the tensile maximum principal stress along the fibre–matrix interface and the negative residual stress in the *y*-direction at the left-top corner of the quarter unit cell in Fig. 3a. For high resin strength, there is an area with a low ratio of shear to normal loading for which the residual stress appears to be beneficial as shown in Fig. 16b. In this area, the ratio of shear to normal loading is less than 1 and the loading can be regarded as equivalent to the transverse tensile loading for which the residual stress is beneficial for relatively high resin strength (see Figs. 10 and 15b).

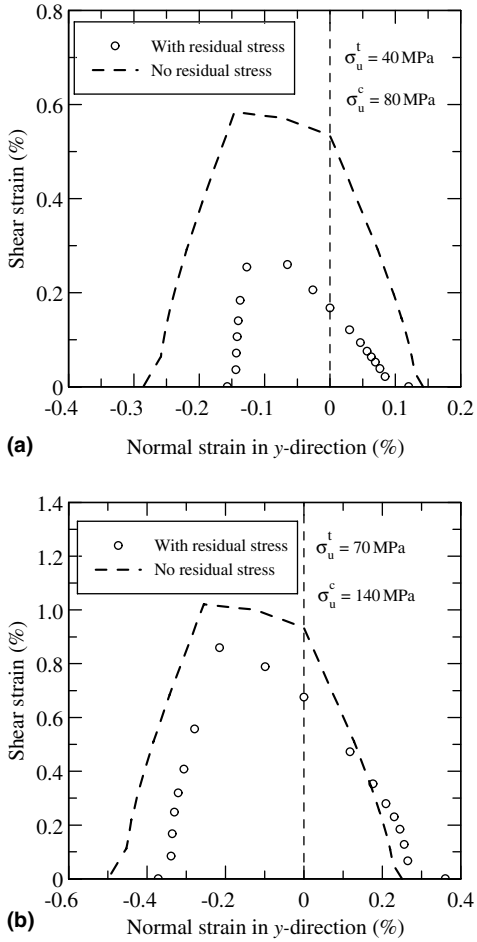

Fig. 16. Failure envelopes for combined transverse normal and shear loading: (a) $\sigma_u^c = 2\sigma_u^t = 80$ MPa and (b) $\sigma_u^c = 2\sigma_u^t = 140$ MPa.

5. Conclusions

Residual stress and its effect on transverse failure of fibre-reinforced polymer–matrix composites were studied using a micromechanical unit cell model and the finite element method. Determination of residual stress in polymer–matrix composites should include contributions from both the chemical shrinkage of the resin and the thermal cooling contraction of the fibre and the resin. Analyses considering the thermal cooling stress only may underestimate the overall residual stress during cure.

For tension-dominated transverse loading, residual stress could be detrimental or beneficial depending on the magnitude of the residual stress and the material strength. Specifically, shrinkage is detrimental for relatively low resin strength and beneficial for relatively high resin strength. Residual stress is always detrimental for compression-dominated transverse loading and pure shear loading.

A shifting and contraction of failure envelopes for transverse biaxial normal loading and combined shear and normal loading are predicted by considering the residual stress.

Acknowledgement

This work is funded by the EPSRC of the UK through the Nottingham Innovative Manufacturing Research Centre (NIMRC).

References

ABAQUS 6.5, 2005. Hibbitt, Karlsson and Sorensen Inc, Providence, RI, USA.

Aghdam, M.M., Khojeh, A., 2003. More on the effects of thermal residual and hydrostatic stresses on yielding behaviour of unidirectional composites. Composite Structures 62, 285–290.

Andersson, B., Sjögren, A., Berglund, L., 2000. Micro- and meso-level residual stresses in glass-fibre/vinyl-ester composites. Composites Science and Technology 60, 2011–2028.

Asp, L.E., Berglund, L.A., Talreja, R., 1996. Prediction of matrix-initiated transverse failure in polymer composites. Composites Science and Technology 56, 1089–1097.

Benedikt, B., Kumosa, M., Predecki, P.K., Kumosa, L., Castelli, M.G., Sutter, J.K., 2001. An analysis of residual thermal stress in a unidirectional graphite/PMR-15 composite based on X-ray diffraction measurements. Composites Science and Technology 61, 1977–1994.

Blackketter, D.M., Walrath, D.E., Hansen, A.C., 1993. Modeling damage in a plain weave fabric-reinforced composite material. Journal of Composite Technology Research 15, 136–142.

Dannenberg, H., 1965. Determination of stresses in cured epoxy resins. SPE Journal (July), 669–675.

Flores, F., Gillespie, J.W., Bogetti, T.A., 2002. Experimental investigation of the cure-dependent response of vinyl ester resin. Polymer Engineering and Science 42, 582–590.

Gascoigne, H.E., 1994. Residual surface stress in laminated cross-ply fibre-epoxy composite materials. Experimental Mechanics 34, 27–36.

Gentz, M., Armentrout, D., Rupnowski, P., Kumosa, L., Shin, E., Sutter, J.K., Kumosa, M., 2004a. In-pane shear testing of medium and high modulus woven graphite fiber reinforced/polyimide composites. Composites Science and Technology 64, 203–220.

Gentz, M., Benedikt, B., Sutter, J.K., Kumosa, M., 2004b. Residual stress in unidirectional graphite fiber/polyimide composites as a function of aging. Composites Science and Technology 64, 1671–1677.

Gopal, A., Adali, S., Verijenko, V.E., 2000. Optimal temperature profiles for minimum residual stress in the cure process of polymer composites. Composite Structures 48, 99–106.

Ifju, P.G., Niu, X., Kilday, B.C., Liu, S.C., Ettinger, S.M., 2000. Residual stress measurement in composite using the cure-referencing method. Experimental Mechanics 40, 22–30.

Kesler, O., Matejicek, J., Sampath, S., Suresh, S., Gnaeupel-Herold, T., Brand, P.C., Prask, H.J., 1998. Measurement of residual stress in plasma-sprayed metallic, ceramic and composite coatings. Materials Science and Engineering A 257, 215–224.

Kim, R.Y., Hahn, H.T., 1979. Effect of curing stress on the first ply-failure in composite laminates. Journal of Composite Materials 13, 2–16.

Kim, Y.K., White, S.R., 1998. Cure-dependent viscoelastic residual stress analysis of filament-wound composite cylinders. Mechanics of Composite Materials and Structures 5, 327–354.

Kwon, Y.W., Berner, J.M., 1997. Matrix damage of fibrous composites: effects of thermal residual stress and layer sequences. Computers and Structures 64, 375–382.

Lange, J., Toll, S., Månson, J.-A.E., 1995. Residual stress build-up in thermoset films cured above their ultimate glass transition temperature. Polymer 36, 3135–3141.

Lennon, A.B., Prendergast, P.J., 2002. Residual stress due to curing can initiate damage in porous bone cement: experimental and theoretical evidence. Journal of Biomechanics 35, 311–321.

Li, C., Potter, K., Wisnom, M.R., Stringer, G., 2004. In-situ measurement of chemical shrinkage of MY750 epoxy resin by a novel gravimetric method. Composites Science and Technology 64, 55–64.

Nimmer, R.P., 1990. Fibre–matrix interface effect in presence of thermally induced residual stresses. Journal of Composites Technology and Research 12, 65–75.

Olivier, P., Cottu, J.P., 1998. Optimisation of the co-curing of two different composites with the aim of minimising residual curing stress levels. Composites Science and Technology 58, 645–651.

Oota, K., Saka, M., 2001. Cure shrinkage analysis of epoxy molding compound. Polymer Engineering and Science 41, 1373–1379.

Rendler, N.J., Vigness, I., 1966. Hole-drilling strain gauge method of measuring residual stress. Experimental Mechanics 6, 577–586.

Russell, J.D., 1993. Cure shrinkage of thermoset composites. SAMPE Quarterly (January), 28–33.

Sakaguchi, R.L., Wiltbank, B.D., Murchison, C.F., 2004. Prediction of composite elastic modulus and polymerization shrinkage by computational micromechanics. Dental Materials 20, 397–401.

Soden, P.D., Hinton, M.J., Kaddour, A.S., 1998. Lamina properties, lay-up configurations and loading conditions for a range of fibre-reinforced composite laminates. Composites Science and Technology 58, 1011–1022.

Soden, P.D., Hinton, M.J., Kaddour, A.S., 2002. Biaxial test results for strength and deformation of a range of E-glass and carbon fibre reinforced composite laminates: failure exercise benchmark data. Composites Science and Technology 62, 1489–1514.

Stone, M.A., Schwartz, I.F., Chandler, H.D., 1997. Residual stress associated with post-cure shrinkage in GRP tubes. Composites Science and Technology 57, 47–54.

Stone, M.A., Fink, B.K., Bogetti, T.A., 2000. Thermal-chemical response of vinyl-ester resin. Polymer Engineering and Science 40, 2489–2497.

Sun, C.T., Vaidya, R.S., 1996. Prediction of composite properties from a representative volume element. Composites Science and Technology 56, 171–179.

Sweeting, R.D., Thomson, R.S., 2004. The effect of thermal mismatch on Z-pinned laminated composite structures. Composite Structures 66, 189–195.

Yuan, F.G., Pagano, N.J., Cai, X., 1997. Elastic moduli of brittle matrix composites with interfacial debonding. International Journal of Solids and Structures 34, 177–201.

Zhang, L., Ernst, L.J., Brouwer, H.R., 1998. Transverse behaviour of a unidirectional composite (glass fibre reinforced polyester). Part II. Influence of shrinkage strains. Mechanics of Materials 27, 37–61.

Zhang, Y., Xia, Z., Ellyin, F., 2004. Evolution and influence of residual stress/strains of fiber reinforced laminates. Composites Science and Technology 64, 1613–1621.

Zhao, L.G., Warrior, N.A., Long, A.C., in press. Finite element modelling of damage progression in non-crimp fabric reinforced composites. Composites Science and Technology.